Effects of Loading-Rate on the Fracture Toughness of Epoxy Encapsulants for the LUNAR-A Penetrator

TODO, Mitsugu
Research Institute for Applied Mechanics Kyushu University

TAKAHASHI, Kiyoshi
Research Institute for Applied Mechanics Kyushu University

HIGUCHI, Ken
The Institute of Space and Astronautical Science

https://doi.org/10.15017/6768410

出版情報：九州大学応用力学研究所所報. 121, pp.95-103, 2001-09. Research Institute for Applied Mechanics, Kyushu University

Effects of Loading-Rate on the Fracture Toughness of Epoxy Encapsulants for the LUNAR-A Penetrator

Mitsugu TODO[*1], Kiyoshi TAKAHASHI[*1] and Ken HIGUCHI[*2]

E-mail of corresponding author: *tohdoh@riam.kyushu-u.ac.jp*

(Received July 26, 2001)

Abstract

The mode I fracture behaviors of different types of epoxy encapsulants used for the LUNAR-A penetrators were investigated at different loading rates. Mode I fracture toughnesses, K_{IC}, of neat epoxy systems (CY1 and CY2 are tough epoxies and 828 a rubber toughened epoxy) and their glass bubbles filled systems (CY1K, CY2A, CY2K and 828D) were measured in a wide range of loading rates from 10^{-5} to 8 m/s using three different types of testing systems. It is interesting to note that K_{IC} of the neat resins decreased as loading rate increased; on the other hand, K_{IC} of the composites increased with increase of loading rate. CY2 exhibited very ductile fracture behavior and possessed the highest K_{IC} at low rates; however, its glass filled systems, CY2A and CY2K, became brittle and their K_{IC} values were similar to that of 828D, although K_{IC} of 828 was much lower than that of CY2 at low rates. It is also seen that K_{IC} of 828D was the largest at the highest impact rate although the impact K_{IC} of the matrix 828 was lower than those of the other neat systems. A toughening mechanism due to interfacial debonding is considered to result in the high K_{IC} of 828D at impact rates. The effects of loading rate on K_{IC} are discussed on the basis of the mode I fracture test results at different loading rates. Fracture micromechanisms are also characterized on the basis of the microscopies performed using optical and scanning electron microscopes.

Key words : , *Glass particle reinforced composite, Rubber toughened epoxy, Mode I fracture, Impact*

1. Introduction

The Japanese lunar penetrator mission, LUNAR-A, has been projected by The Institute of Space and Astronautical Science (ISAS) [1)]. The mission aims to investigate the lunar interior using seismometers and heat-flow probes installed in the penetrators and will be launched by ISAS in 2002. Two penetrators will be deployed on the lunar surface as shown in Fig. 1; one on the nearside and another on the farside. The penetrators contain a two-component seismometer and a heat-flow probe together with other supporting instruments such as a tiltmeter and an accelerometer. They also contain various electronics, including the data-handling unit, communication system and batteries as power source for all the instruments. Those scientific instruments and electronics are encapsulated by epoxy based materials. During the first stage of the development of the penetrators, a tough epoxy was selected as the base of the encapsulant, which was a glass bubbles filled epoxy composite; however, after a preliminary penetrating test was performed, it was found that the instruments were damaged due to the failure of the encapsulant. A committee was organized to investigate the source of the accident, and after several meetings were held, three different types of epoxies (two new epoxies with the original) were newly selected as the candidates. During the mission, the penetrators are expected to be subjected to different types of loading from static to impact; therefore, the fracture behavior of the base epoxies and the encapsulants at different loading rates must be understood to ensure the safety of the penetrators.

In the present study, the mode I fracture behavior of three kinds of the base epoxies and four kinds of glass bubbles filled epoxy composites were investigated. Mode I fracture toughness, K_{IC}, of those materials were measured at different loading rates ranging from 10^{-5} to 8 m/s. A servohydraulic testing machine was used for the fracture tests at low loading rates up to 10^{-2} m/s, and an instrumented drop weight tester and a modified SHPB impact testing system were utilized to measure the impact K_{IC} at higher loading rates. In this paper, the

*1 Research Institute for Applied Mechanics, Kyushu University

*2 The Institute of Space and Astronautical Science.

Fig. 1 LUNAR-A penetrator.

effects of loading rate on K_{IC} are discussed on the basis of the experimental results. Fracture micromechanisms are also characterized on the basis of the microscopies performed using optical and scanning electron microscopes.

2. Experimental

2.1 Materials and specimen

Three different kinds of epoxy systems, CY1, CY2 and 828, were selected as the bases of the encapsulants for the LUNAR-A penetrator. CY1 is the original base epoxy and CY2 and 828 are newly selected epoxies. CY1 and CY2 are tough epoxies and 828 is a rubber toughened epoxy. The combinations of epoxy, hardener and modifier are as follows:

CY1: CY1005 + HY1006
CY2: CY232 + XNH4451
828: EPON828 + CTBN1300x8(10) + DEA

where CY1005 and CY232 are epoxy resins and HY1006 and XNH4451 are hardeners produced by Ciba-Geigy, Japan, Ltd. EPON828 and DEA are a conventional epoxy resin and hardener, respectively, produced by Shell Chemical Co. CTBN1300x8 is an elastomer produced by B. F. Goodrich Co., which has widely been used to toughen brittle epoxies. The CTBN content was 10 phr. The constitutions of glass bubbles filled epoxy composites are as follows:

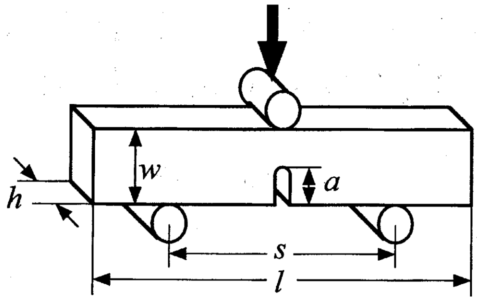

Fig. 2 Geometry of SENB specimen.

CY1K: CY1005 + K15(16.7) + HY1006
CY2K: CY232 + K15(22.8) + XNH4451
CY2A: CY232 + A16(22.8) + XNH4451
828D: EPON828 + CTBN(10) + D32(28) +DEA

where K15, A16 and D32 are glass bubbles fillers produced by 3M Co. The surface of A16 is treated by silane and the comparison between CY2K and CY2A was made to assess the effect of glass surface treatment on their fracture properties. The numbers in parentheses with the glass fillers represent their weight fractions.

For each material, plates of 4mm thick were fabricated on the basis of the following cure condition:

CY1005: 23℃, 72hours → Heating for 1 hour
→ 60℃, 6hours
CY232: 25℃, 5hours → Heating for 1 hour
→ 60℃, 6hours
EPON828: 25℃, 48hours → Heating for 1 hour
→ 60℃, 30hours

The relatively low curing temperature 60℃ was due to the low heat resistibility of the instruments installed in the penetrator. Single edge notch bending (SENB) specimens were machined from the plates and the geometry is shown in Fig. 2.

2.2 Mode I fracture test at low rates

Mode I fracture tests at low displacement rates from 1 to 10^3mm/min (corresponding to 10^{-5} – 10^{-2}m/s) were performed using a servo-hydraulic testing machine with the use of a digital recorder. The mode I fracture toughness, K_{IC}, was then evaluated by using:

$$K_{IC} = f(x)\frac{P_C}{h\sqrt{w}}, \quad x = a/w \tag{1}$$

where P_C is a critical load, h specimen thickness, w specimen depth and a crack length as shown in Fig. 2. The geometrical correction factor $f(x)$ is given by:

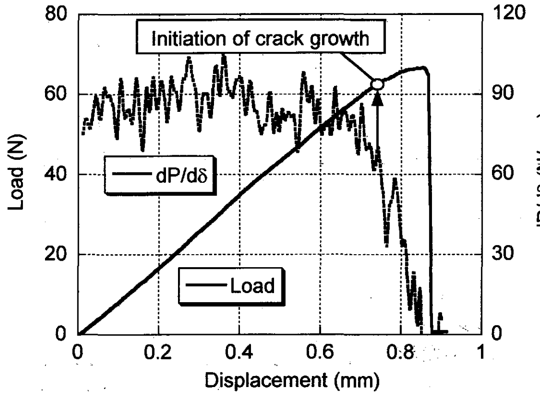

Fig. 3 Determination of the initiation of crack growth.

$$f(x) = 6x^{1/2} \frac{1.99 - x(1-x)(2.15 - 3.93x + 2.7x^2)}{(1+2x)(1-x)^{3/2}} \quad (2)$$

The critical load, P_C, was defined as the load at which the initiation of crack propagation occurred. In the present study, the variation of specimen stiffness, $dP/d\delta$, where δ is the loading-point displacement, was utilized to determine the initiation of crack growth as shown in Fig. 3. P_C was defined as the load at which $dP/d\delta$ suddenly started to decrease. For CY2 exhibiting extensive ductility at low loading rates, the maximum load, P_{max}, was simply chosen as P_C, because its $dP/d\delta$ curves did not show sudden decreases.

2.3 Mode I fracture test at impact rates

An instrumented drop weight impact test system [2)3)] was used to perform mode I fracture tests at a low impact rate of 1.5m/s. In this test system, load is measured using a piezoelectric load cell and stored in PC through a wave memory. It was assumed that quasi-static analysis could be applied for the K_{IC} evaluation at the low impact rate with the use of viscoelastic sheet at the impact points, which reduced dynamic effects dramatically. Thus, Eq.(1) was used to calculate K_{IC} and P_C was assumed to be equivalent to the maximum load, P_{max}.

A modified split Hopkinson pressure bar (SHPB) test system[4)5)] was used to perform mode I fracture tests at high loading rates of 7-9 m/s. The SHPB system is shown in Fig. 4. The striker, input and output bars are made of 2017 aluminum alloy rods of 15 mm diameter, and their lengths are 400 mm, 1500 mm and 1500 mm, respectively. Strains are measured at the positions shown in the figure. Similar SHPB systems have been used to study the impact fracture behaviors of metals and composites[6-8)].

In general, the deformation behavior of a bending specimen under impact loading is noticeably different from that under static loading; therefore, numerical simulation such as dynamic finite element analysis has to be made to evaluate its dynamic bending properties [6)7)]. However, the use of soft metal buffer in the dynamic mode II interlaminar fracture toughness tests of composite laminates[8)] suggests the applicability of a quasi-static analysis to the present impact test results. In the present study, a silicon rubber sheet buffer of 1.5 mm thick was placed between the striker and input bars. It was presumed that the deformation under impact

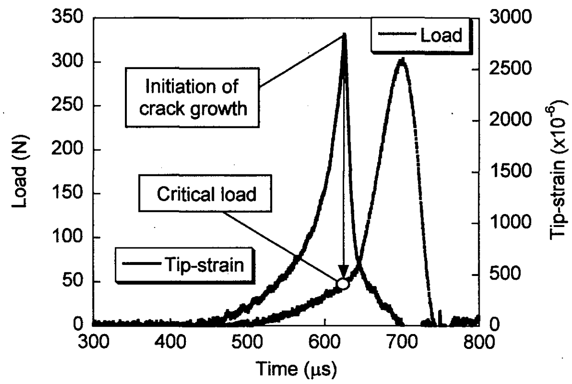

Fig. 5 An example of SHPB test data.

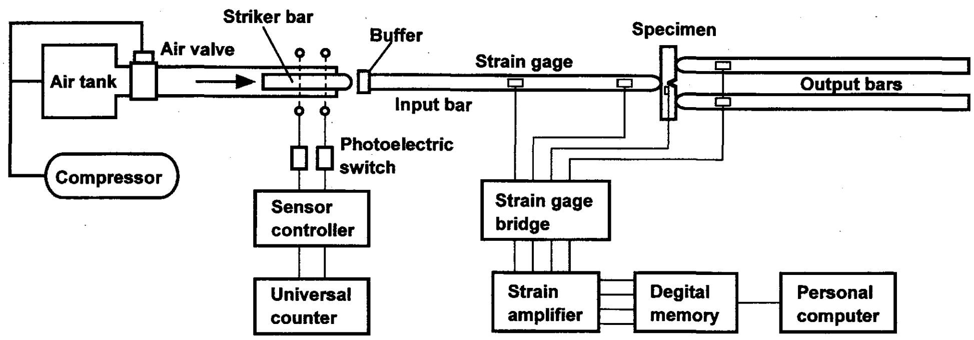

Fig. 4 SHPB impact testing system.

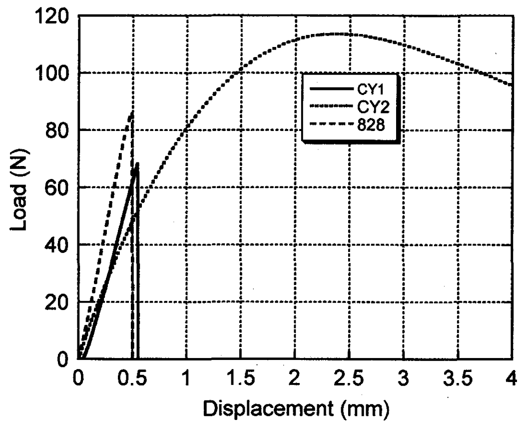

(a) 10mm/min

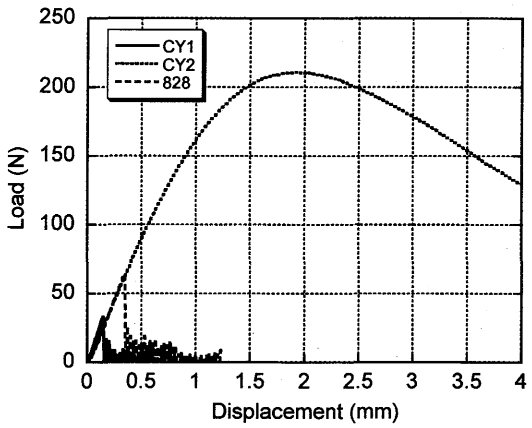

(b) 10^3mm/min

Fig. 6 Load-displacement curves of base epoxy resins.

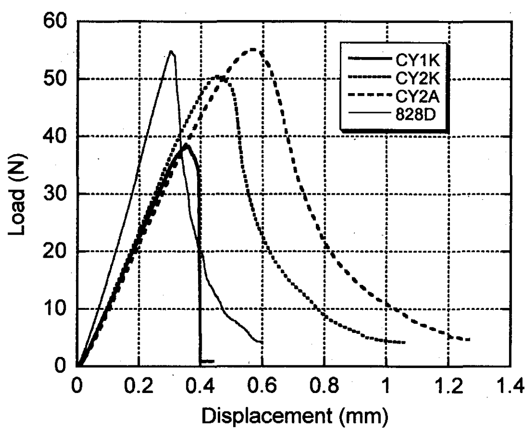

(a) 10mm/min

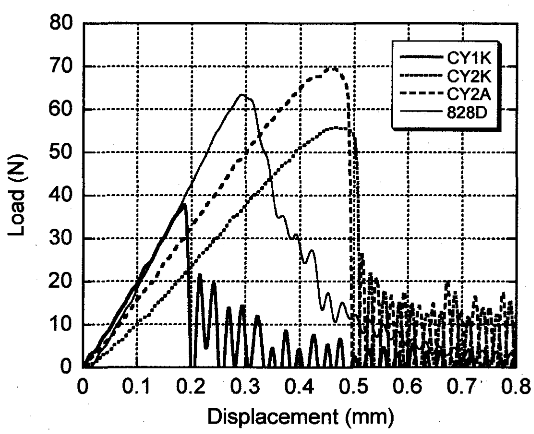

(b) 10^3mm/min

Fig. 7 Load-displacement curves of glass bubbles filled epoxy resins.

bending with the use of the viscoelastic buffer was approximately equivalent to that under quasi-static bending. On the basis of this presumption, Eqs. (1) and (2) were used to evaluate mode I fracture toughness with the use of the transmitted force-displacement curves. For each specimen, the initiation of crack growth was detected at the point where crack-tip strain suddenly decreased as shown in Fig. 5. P_C was then determined at the initiation point.

2.4 Microscopic observation

The fracture surfaces of the tested specimens created at different loading rates were observed using an optical microscope and a scanning electron microscope (SEM) to characterize the effects of loading rate on the fracture micromechanisms.

3. Results

3.1 Load-displacement curves at low rates

Fig. 6 shows the load-displacement curves of the base epoxies at 10 and 10^3mm/min. It is clearly seen that CY2 was much tougher than the other epoxies. P_{max} of CY2 tended to increase with increase of loading rate up to 10^3mm/min; on the other hand, P_{max} of CY1 and 828 tended to decrease as loading rate increased. Fig. 7 shows the load-displacement curves of the glass bubbles filled epoxy composites at 10 and 10^3mm/min. It is noted that the predominance of CY2 suppressed in its glass bubbles filled systems at both loading rates. P_{max} of 828D was almost equivalent to those of CY2K and CY2A, although the corresponding maximum displacement of 828D was smaller than those of CY2K and CY2A. P_{max} of CY1K was the lowest of all the materials.

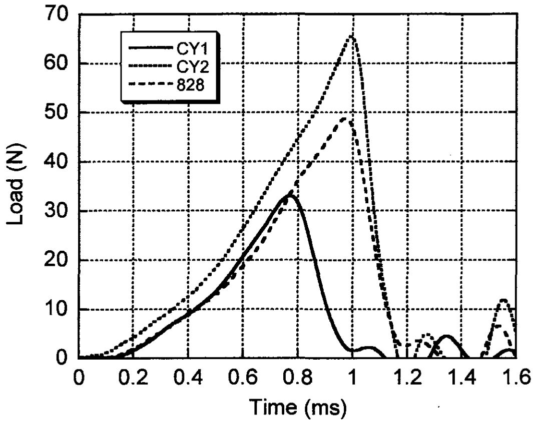

(a) Base epoxy resins

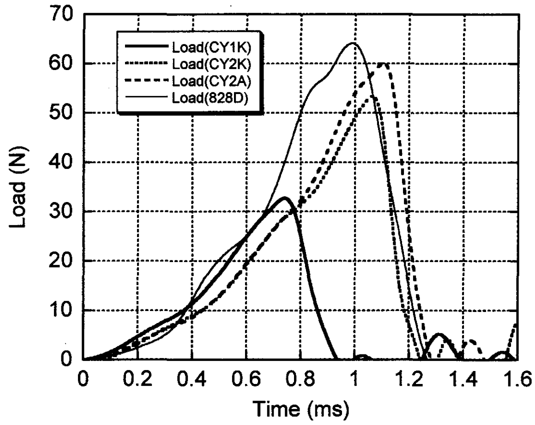

(b) Glass bubbles filled systems

Fig. 8 Load—time curves recorded at 1.5m/s.

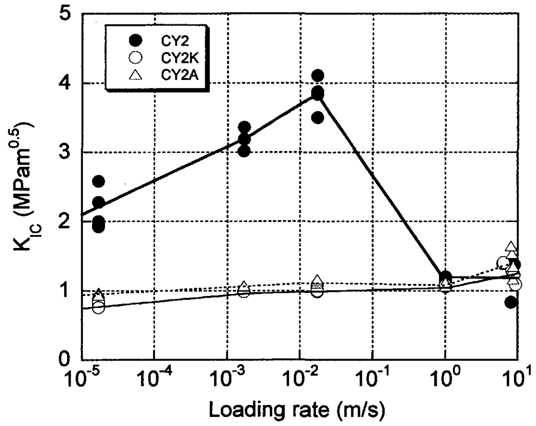

(a) Base epoxy resins

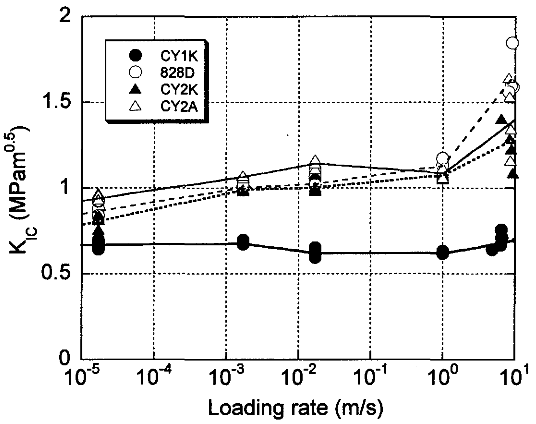

(b) Glass bubbles filled systems

Fig. 9 Loading-rate dependence of K_{IC}.

3.2 Load-time curves at an impact rate

Load-time curves recorded at 1.5m/s are shown in Fig. 8. It is interesting to note that the difference between CY2 and the others became small, suggesting that the high fracture resistance caused by the ductile nature of CY2 was dramatically reduced at impact loading rate. CY1 and CY1K exhibited the lowest impact resistance; on the other hand, 828 and 828D possessed much better impact resistances, which were almost identical to CY2 and its composite systems.

3.3 Mode I fracture toughness

The loading-rate dependences of K_{IC} are shown in Fig. 9. It is seen from Fig. 9(a) that K_{IC} of CY2 increased with increase of loading rate up to 10^3mm/min, and then suddenly decreased at impact rates; as a result, K_{IC} of CY2 became equivalent to those of CY1 and 828. Fig. 9(b) shows that K_{IC}'s of 828D, CY2K and CY2A increased with increase of loading rate, and the difference between them was very small. K_{IC} of CY2A was slightly better than that of CY2K as a result of surface treatment. On the other hand, K_{IC} of CY1K appeared to be almost independent of loading rate. K_{IC} values and their rate dependences of the base epoxies can be compared with their composites in Fig. 10. It is interesting to see that K_{IC} of 828 tended to decrease as loading rate increased, although that of 828D increased with increase of loading rate. Fig. 10(b) exhibits that the high fracture toughness of CY2 did not reflect on those of CY2K and CY2A at the low rates from 10 to 10^3mm/min; however, K_{IC} of CY2 was almost equivalent to those of CY2A and CY2K at the impact

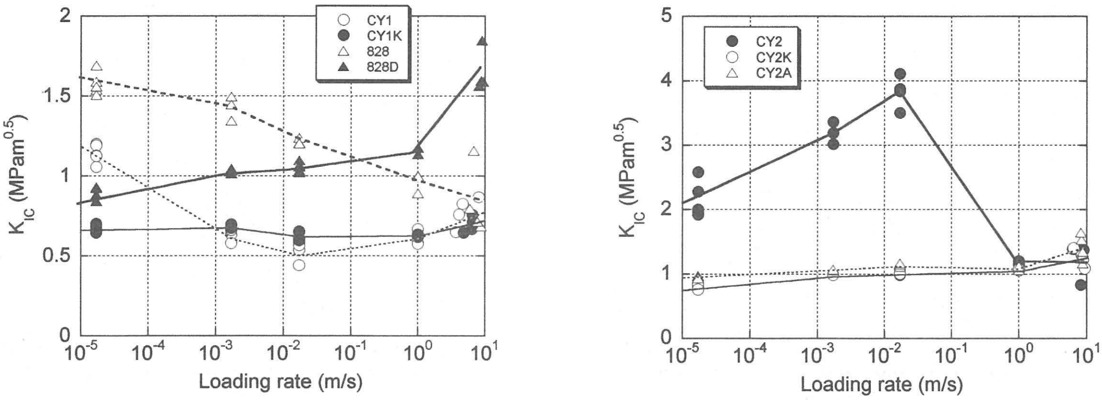

(a) CY1 and 828 (b) CY2

Fig. 10 Comparison between the base epoxies and their composite systems.

rates, indicating that the loading-rate dependence of K_{IC} of CY2 did not have an influence on those of its composite systems.

Thus, the newly selected epoxies, CY2 and 828, for encapsulating possessed better fracture toughness than the original base epoxy, CY1, at low loading rates. The glass bubbles filled epoxy systems, CY2K, CY2A and 828D exhibited much better fracture toughness than the original encapsulant, CY1K, at all loading rates examined.

3.4 Microscopic characterization

Fracture surface morphology of CY2 at three different loading rates is shown in Fig. 11. It is clearly seen that the fracture surfaces were very rough at the low rates, indicating ductile fracture; on the other hand, the surface became very smooth at the impact rate, suggesting brittle fracture at high loading rate. Thus, this morphology reveals that a ductile-brittle transition existed on the fracture behavior. It is also understood that the ductile fracture behavior resulted in the high K_{IC} of CY2 at low loading rates, and the dramatic reduction of K_{IC} at impact rates corresponded to the smooth fracture surface. SEM photographs of the fracture surfaces of 828 are shown in Fig. 12. It is seen that the fracture surface at 10^3mm/min was smoother than that at 10mm/min, corresponding to the decrease of K_{IC} with increase of loading rate. Fracture of CTBN rubber particles was also observed.

SEM photographs of the fracture surfaces of 828D are shown in Fig. 13. Fracture of CTBN rubber particles were observed. It should be noted that the interfacial failure between the glass bubbles and the matrix was observed at 10^3mm/min, although the interfacial bonding was fairly good at the lower rate of 10mm/min. It is thus considered that a toughening mechanism due to interfacial debonding might result in the increase of K_{IC} with increase of loading rate. A theory explaining the toughening mechanism due to microcrack shielding is

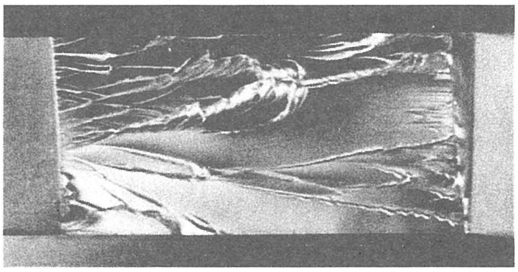

(a) 10mm/min

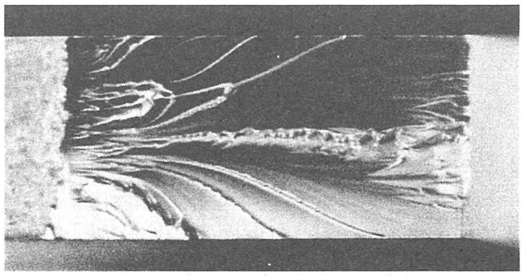

(b) 10^3mm/min

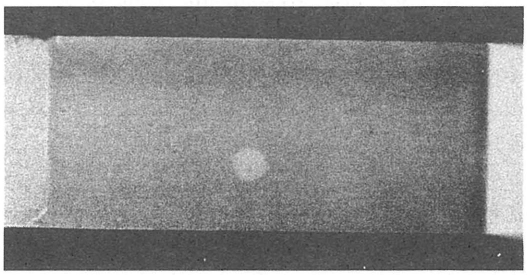

(c) 8m/s

Fig. 11 Fracture surface morphology of CY2

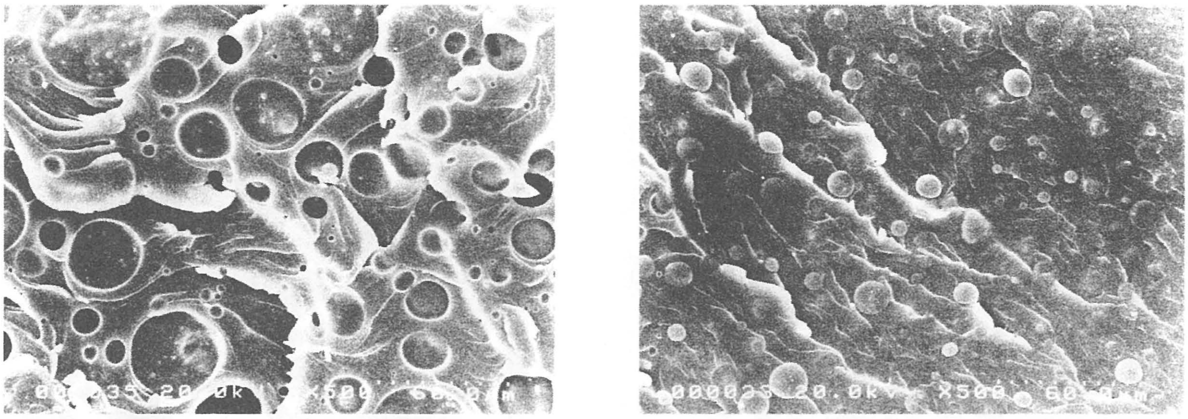

(a) 10mm/min (b) 10^3mm/min

Fig. 12 SEM photographs of the fracture surfaces of 828.

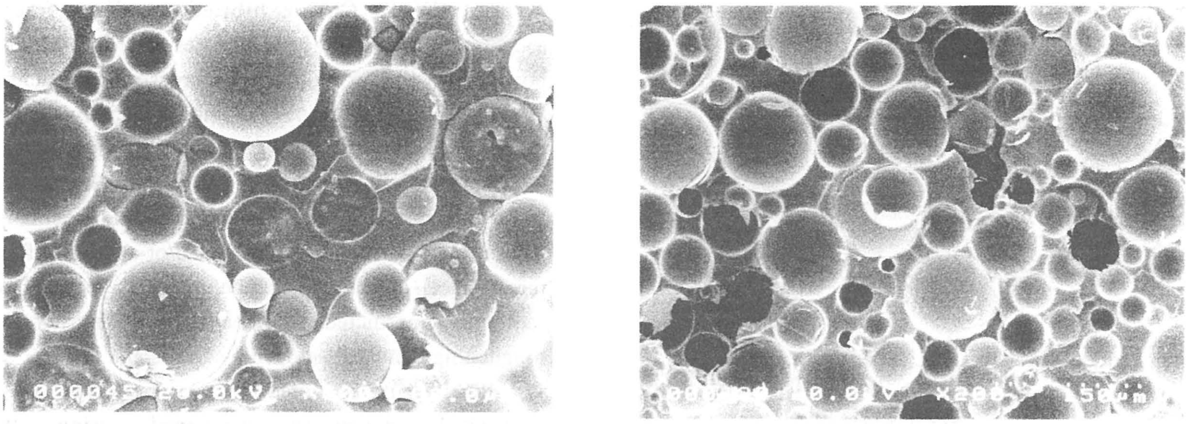

(a) 10mm/min (b) 10^3mm/min

Fig. 13 SEM photographs of the fracture surfaces of 828D.

presented in the following section. SEM photographs of the fracture surfaces of CY2A are shown in Fig. 14. Interfacial failure observed in 828D was not seen in this material, although K_{IC} of CY2A increased with increase of loading rate. The detail of the loading-rate effect on K_{IC} of CY2A will be throughly investigated in the subsequent studies.

3.5 Microcrack toughening mechanism

If microcracking generates within a process zone ahead of a crack-tip, the measured toughness, K_C^∞, becomes larger than the base toughness, K_C, of the material. Evans and Faber presented a simple theory to explain this toughening mechanism due to microcracking[9]. The relation between K_C^∞ and K_C can be expressed by:

$$K_C^\infty \approx (E/E_1)^{1/2}(1-f_s)K_C \quad (3)$$

where E is the Young's modulus of the material without microcracks, E_1 the modulus at microcrack saturation condition, and f_s is the volume fraction of microcracks. The ratio E_1/E can be given by a function of f_s:

$$E_1/E \approx 1-16(1-\nu_1^2)(10-3\nu_1)f_s/45(2-\nu_1) \quad (4)$$

where ν_1 is the Poisson's ratio at microcrack saturation condition and is given by:

$$\nu_1 = \nu(1-16f_s/9) \quad (5)$$

where ν is the Poisson's ratio of the material without microcracks. If we now assume that f_s in 828D can be

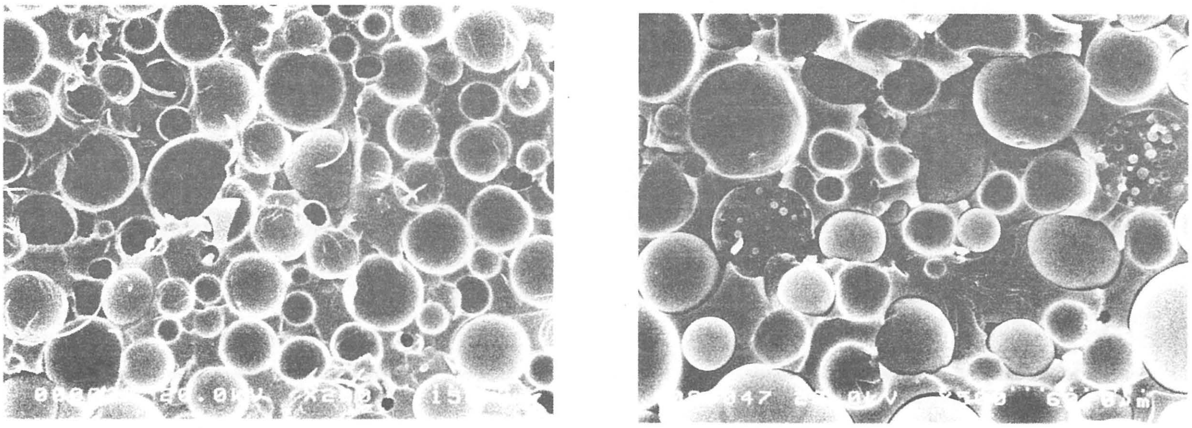

(a) 10mm/min

(b) 10^3mm/min

Fig. 14 SEM photographs of the fracture surfaces of CY2A.

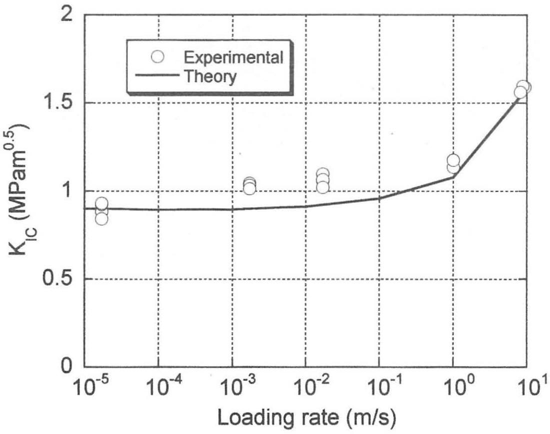

Fig. 15 Comparison between a microcrack toughening theory and experimental results of 828D.

expressed as a linear function of the logarithm of loading rate, v, such that:

$$f_s = a \ln v + b \tag{6}$$

and choose a=0.0863 and b=0.4317, corresponding to f_s=0 at 10^{-5}m/s and f_s=0.518 at 10m/s, then using Eqs.(3)-(6), we obtain a theoretical curve shown in Fig. 15. The theory predicted the experimental results reasonably well.

4. CONCLUSIONS

Tough epoxy, CY2, and three types of glass bubbles filled epoxies, CY1K, CY2A and 828D have been selected as the encapsulants for the penetrators in the LUNAR-A project. It was found that all the new systems, CY2, CY2A and 828D, were tougher than the original system, CY1K. CY2 exhibited excellent fracture toughness K_{IC} at low loading rates up to 10^3mm/min; however, K_{IC} of CY2 suddenly decreased at impact rates. 828D showed superior performance especially at impact loading rates. K_{IC} of the glass filled systems increased with increase of loading rate. This phenomena appeared to be closely related to the crack shielding mechanisms caused by interfacial debonding and/or another different mechanisms. The loading-rate effect of K_{IC} of 828D was reasonably predicted by means of a microcracking toughening theory developed by Evans and Faber.

Finally, it is noted that a prototype of the LUNAR-A penetrator developed using these encapsulants successfully cleared a penetrating test conducted in May, 2000, in the United States.

References

1) ISAS home page, http://www.isas.ac.jp/e/enterp/missions/lunar-a/
2) Todo, M., T. Nakamura and K. Takahashi. 1999. "Mode II Interlaminar Fracture Behavior of Fiber Reinforced Polyamide Composites under Static and Dynamic Loading Conditions," J. Rein. Plas. Comp., 18(15):1415-1427.
3) Todo, M., T. Nakamura and K. Takahashi. 2000. "Effects of Moisture Absorption on the Dynamic Interlaminar Fracture Toughness of Carbon/Epoxy Composites," J. Comp. Mater., 34(8): 630-648.
4) Todo, M., and K. Takahashi. 1999. "Dynamic Fracture Behavior of Interlayer-Toughened Graphite/Epoxy Composite under Bending Loading, " Proc. of the 14th Annual Technical Conference on Composite Materials, September

27-29, Fairborn, Ohio, pp.131-140.

5) Todo, M. and K. Takahashi. 2001. "Displacement-Rate Dependence of the Bending Fracture Behavior of Interlayer-Toughened Carbon/Epoxy Composite," Materials Science Research International, Special Technical Publication-2: 266-270.
6) Yokoyama, T., and K. Kishida. 1989. "A Novel Impact Three-Point Bend Test Method for Determining Dynamic Fracture-Initiation Toughness," Exper. Mech., 29:188-194.
7) Yokoyama, T. 1993. "Determination of Dynamic Fracture-Initiation Toughness using a Novel Impact Bend Test Procedure ," J. Press. Vess. Tech., 115:389-397.
8) Kusaka, T., M. Hojo, S. Ochiai and T. Kurokawa. 1999. "Rate-Dependent Mode II Interlaminar Fracture Behavior of Carbon-Fiber/Epoxy Composite Laminates," Mater. Sci. Res. Inter., 5(2): 98-103.
9) Evans, A.G., and K. T. Faber. 1984. "Crack-Growth Resistance of Microcracking Brittle Materials," J. American Ceramic Soc., 67(4): 255-260.